Eccentric Birth Rings, Asymmetric Debris Disks, and HD 15115

Joseph M. Hahn
Space Science Institute
Austin, TX

Introduction

Debris disks are the dusty circumstellar disks that are known to orbit a number of nearby stars. These dust disks are transient and must also be replenished, since collisions as well as stellar radiation forces tend to drain a disk of its dust. Many of these disks appear to be sustained by an unseen 'birth ring' of planetesimals whose collisions generate the observed dust. Small dust can then drift inwards of the ring due to Poynting-Robertson drag, with even smaller dust grains being lofted outwards into wide orbits (~ 100's of AU) by radiation pressure (Strubbe & Chiang 2006). These two different transport mechanisms also cause the dust-disk's optical depth to change at the birth-ring's radius a_r. And when such a disk is viewed edge on, as for AU Mic and β Pic, this also causes the disk's surface brightness to fall of rapidly as $\propto r^{-3.5}$ at projected distances of $r \gg a_r$, and less rapidly at $r \ll a_r$ (Strubbe & Chiang 2006); see also Fig. 1.

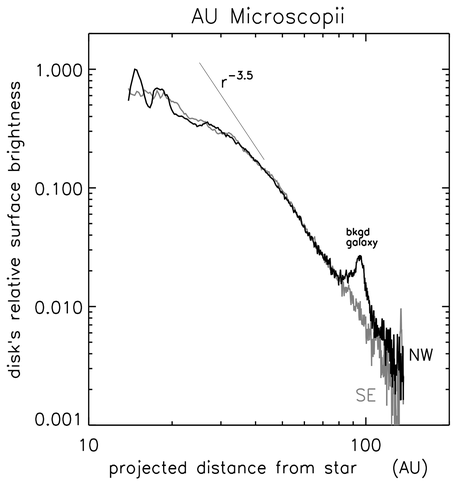

FIGURE 1: Surface brightness profiles of the AU Mic debris disk, plotted versus projected distance from the central star, along its northwest (NW) and southeast (SE) ansae. These profiles are extracted from an optical HST image provided by John Krist, also described in Krist et al (2005). Note that the outer disk's profile varies as $r^{-3.5}$ at $r \gg 43$ AU, while its inner profile has a shallower slope, which suggests the presence of a birth ring of planetesimals of radius $a_r \simeq 43$ AU (Strubbe & Chiang 2006). Although it is hard to see in this figure, the NW ansa is $\sim 2\times$ brighter than the SE ansa at distances of $r \gtrsim 100$ AU (Krist et al 2005).

Also note that these dust-disks are often asymmetric. For instance, the northwest ansa of the AU Mic debris disk is ~ 2 brighter than the southeast ansa at projected distances of $r \gtrsim 100$ AU (Krist et al 2005; see also Fig. 1). Similarly, the NE ansa of the β Pic dust-disk is $\sim 50\%$ brighter than its SW half at projected distances of $r \gtrsim 200$ AU (from HST observations provided by David Golimowski). And the disk orbiting HD 15115 is the most extreme example of an asymmetric dust-disk, since its western ansa extends about twice as far as its eastern one; see Fig. 2.

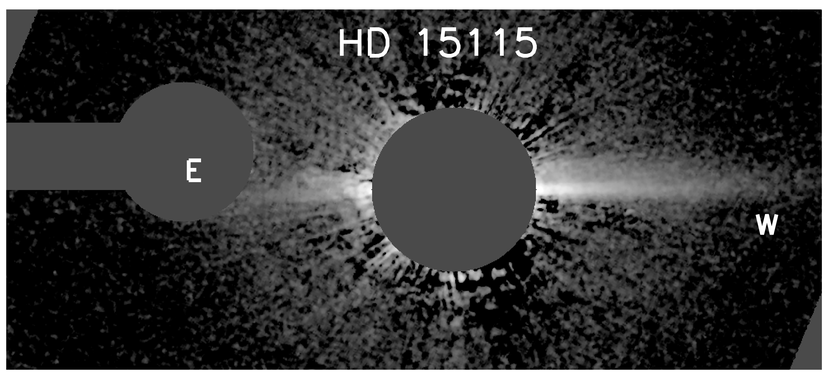

FIGURE 2: Optical HST image of the debris disk orbiting HD 15115, from Kalas et al (2007). This disk's western ansa extends beyond the detector's edge at $r \sim 500$ AU from the star, while its eastern ansa is seen only out to $r \sim 300$ AU, where it is partially masked by other occulting disks and fingers in the HST's optics (greyed regions).

We suspect that the large-scale asymmetries that are routinely seen in these debris disks are due to the birth ring's eccentricity. Note that when the birth ring is eccentric, the dust size-threshold for blow-out via radiation pressure becomes sensitive to the longitude in the ring where the dust is generated. As the following shows, this will cause one side of the disk to be overdense with the smaller grains that tend to dominate a disk's optical depth, giving the disk a 'lopsided' appearance.

Dust orbits

An orbiting dust grain is characterized by its dimensionless size parameter $\beta = 3L_\star/16\pi GM_\star \rho R c$, which is the ratio of radiation pressure to stellar gravity, and all symbols have their usual meaning, so grains with smaller radii R have larger β.

A dust grain is produced by a collision among planetesimals in the birth ring, and that grain's orbit is characterized by its energy integral E, its angular momentum integral L, and its Laplace-Runga-Lenz (LRL) vector $\mathbf{A}$, where

$$E = -\frac{GM_\star(1-\beta)}{2a} = \frac{1}{2}v_r^2 - \frac{GM_\star(1-\beta)}{r_r}, \qquad (1)$$

$$L = \sqrt{GM_\star(1-\beta)a(1-e^2)} = r_r^2\dot{\theta}_r \qquad (2)$$

$$\text{and} \quad \mathbf{A} = \frac{\dot{\mathbf{r}}_\mathbf{r} \times (\mathbf{r}_\mathbf{r} \times \dot{\mathbf{r}}_\mathbf{r})}{GM_\star(1-\beta)} - \frac{\mathbf{r}_\mathbf{r}}{r_r}. \qquad (3)$$

The LRL vector is particularly useful here since its magnitude is the grain's eccentricity e and it points towards the grain's periapse (Goldstein 1980). Since the parent planetesimal and its dust grain have the same positions and velocities r_r, v_r, and $r_r\dot{\theta}_r$ at the moment of creation, the above can be used to solve for the grain's semimajor axis a, eccentricity e, and longitude of periapse $\tilde{\omega}$,

$$a = \frac{(1-\beta)a_r}{1-2\beta a_r/r_r}, \qquad e = \sqrt{1 - \frac{a_r}{a}\left(\frac{1-e_e^2}{1-\beta}\right)}, \quad \text{and} \quad \tan\tilde{\omega} = \frac{\beta\sin\theta_r}{\beta\cos\theta_r + e_r} \qquad (4)$$

where a_r and e_r are the birth-ring's orbit elements, and (r_r, θ_r) are the polar coordinates in the ring. Note that when the birth-ring's eccentricity $e_r \to 0$, we recover the familiar result that $e \to \beta/(1-\beta)$ and $a \to a_r/(1-e)$. Inserting the orbit elements of Eqn. (4) into the ellipse equation then yields the dust grain's trajectory

$$r(\theta;\beta,\theta_r) = \frac{a_r(1-e_r^2)}{1-\beta[1-\cos(\theta-\theta_r)]+e_r\cos\theta}, \qquad (5)$$

which is controlled by the grain size β and the longitude θ_r where the grain was formed.

Figure 3 illustrates the range of trajectories that result for grains having a variety of sizes β. For instance, dust having $\beta < (1-e_r)/2$ can be launched from all longitudes within the birth ring and still stay bound to the system such that $a > 0$; see upper Fig. 3. Note also that trajectories tend to be elongated towards the birth-ring's apoapse, *ie* towards the left side in Fig. 3. This is due to the dust grains' higher velocities when launched from the birth-ring's periapse (right side of Fig. 3).

Smaller dust grains having even larger β can only stay bound to the star when launched at longitudes nearer the ring's longitude of apoapse. This is due to the birth-ring's lower orbital velocity there; see insets to Fig. 3. Smaller dust grains also travel out to greater distances from the central star, while larger dust grains are confined nearer the birth ring. Also note that all dust having $\beta > (1+e_r)/2$ have $a < 0$, are not bound, and quickly leave the system.

Lastly, note that all of the patterns seen here at non-axisymmetric; many of the trajectories tend to be elongated towards the birth-ring's apoapse (to the left of Fig. 3), while the dust streamlines tend to be most dense towards the ring's periapse (to the right). Also it is the latter effect that tends to make the circumstellar debris disk overdense and thus brighter in the direction of the birth ring's periapse.

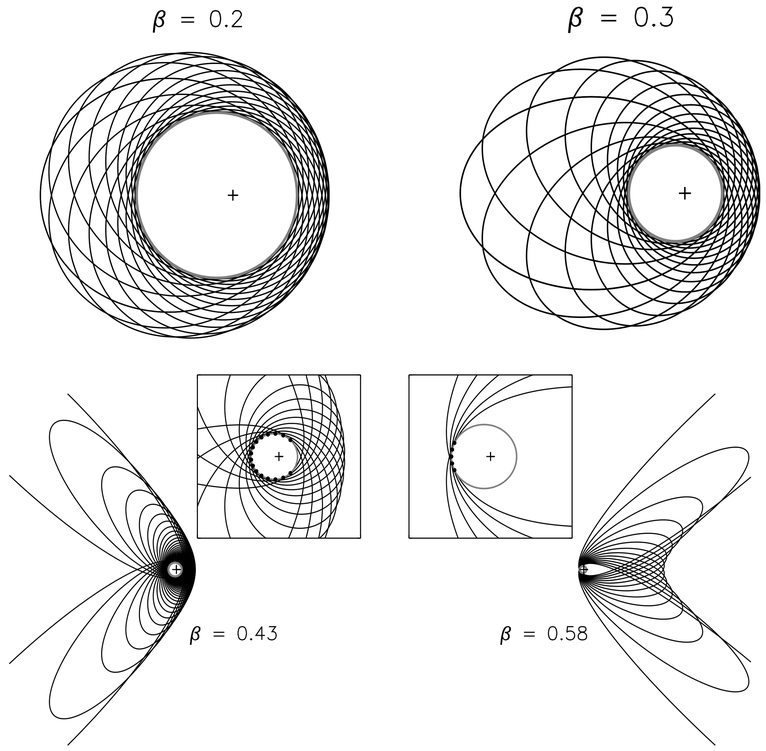

FIGURE 3: Dust trajectories for grains of size β launched at discrete longitudes withing an eccentric birth ring. The birth ring has eccentricity $e_r = 0.2$, and is indicated by the grey ellipse whose size also provides the spatial scale for each figure. A cross denotes the central star. Dust having sizes $0.4 < \beta < 0.6$ are only bound to the system when launched from longitudes nearer the ring's apoapse (to the left in each figure), due to the parent body's lower velocity there. This is indicated in the inset figures that zoom in on the birth ring, which uses dots to indicate those longitudes in the ring that can generate bound dust.

Disk optical depth and surface brightness

Since the trajectories of all dust are given by Eqn. (5), it is straightforward (but tedious) to derive an analytic expression for the number density of dust of radius R at any site in the disk:

$$dn(r,\theta;R) = \frac{dN}{dR}g(r,\theta;R)dR \qquad (6)$$

where $dN/dR \propto R^{-q}$ is the grain's differential size distribution (assumed here to be a power law), and $g(r,\theta;R)$ is the dust grain's spatial density distribution. The total optical depth at any site in the disk is

$$\tau(r,\theta) = \int_{R_{\min}}^{R_{\max}} \pi R^2 dn \qquad (7)$$

where $R_{\min}$ and $R_{\max}$ are the sizes of the smallest and largest grains that can be lofted to site (r,θ) by radiation pressure. A map of the disk's surface brightness $B(r,\theta)$ is then constructed via

$$B(r,\theta) = C\int_{\text{LOS}} \frac{\tau(r,\theta)\psi(\phi)d\ell}{r^2}, \qquad (8)$$

where the integration proceeds along the line-of-sight (LOS) through the disk, and it is assumed that the disk is seen via reflected starlight (thus the r^{-2} factor). The constant C depends on quantities like the stellar luminosity and the total cross section in the dust disk. We also adopt a Henyey-Greenstein function for the dust grain's phase law $\psi(\phi)$, but our results are insensitive to such details when the disk is viewed edge-on. Figure 4 shows examples of such a disk viewed face on and edge on, and Fig. 5 illustrates different outcomes for a variety of birth-ring eccentricities e_r and dust size distributions q.

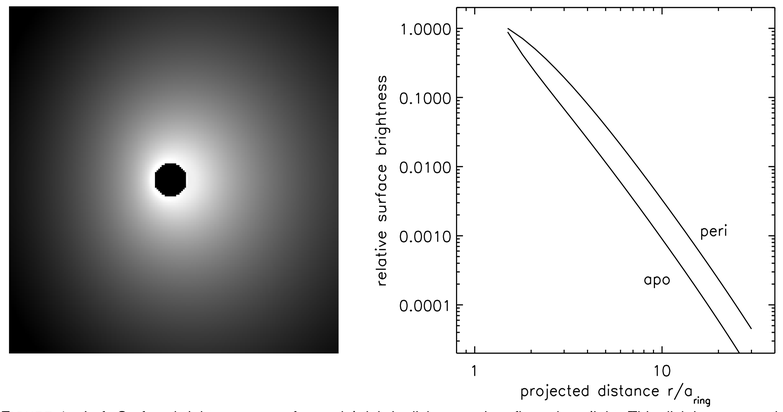

FIGURE 4: *Left:* Surface brightness map of a model debris disk seen via reflected starlight. This disk is generated by a birth ring having eccentricity $e_r = 0.2$ and a steep dust size distribution $q = 8$. The greyscale shows that the resulting disk is lopsided and brighter in the direction of the ring's periapse, which is to the right. *Right:* Surface brightness profiles of this disk as it is viewed edge-on, with the LOS running bottom to top. The ansa in the direction of the ring's periapse is ~ 3.5 times brighter than the apoapse side.

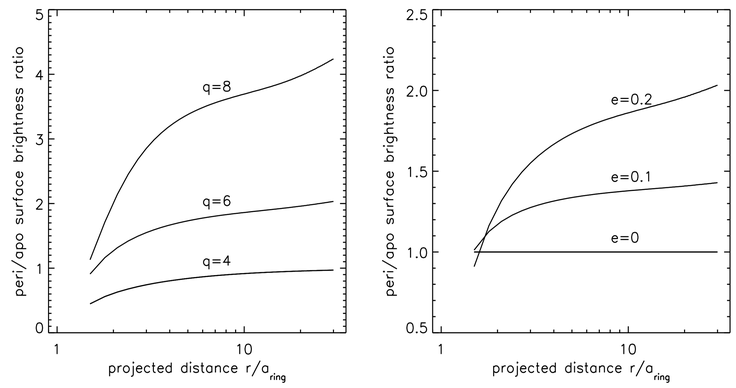

FIGURE 5: *Left:* Model debris disks are generated for a birth ring having $e_r = 0.2$ and a variety of dust size distributions q, and then viewed edge-on with the LOS perpendicular to the birth-ring's long axis. Surface brightness profiles of the disks are then calculated along both of the disk's ansae, *ie* towards the ring's periapse and towards apoapse. Those profiles are ratiod, periapse/apoapse, and plotted versus projected distance from the star. *Right:* Surface brightness profile ratios are shown for a dust disk having a $q = 6$ size distribution and a variety of birth-ring eccentricities e_r.

Findings and implications

- Many debris disks are believed to be dust that is generated by collisions among planetesimals that reside in a birth ring. Radiation pressure then lofts those grains into wide orbits, which results in a broad debris disk (Strubbe & Chiang 2006). Observations show that many such disks are also asymmetric, with one ansa of the disk being brighter than the other by $\sim 50\%$ or more (see Figs. 1–2). It is shown above that this asymmetry can be due to a birth ring that has a modest eccentricity.
- When the birth ring is eccentric, dust grains launched at the ring's periapse are also more eccentric due to the ring's higher orbital velocity there, while grains launched at the ring's apoapse have smaller e (Fig. 3). This results in an asymmetric debris disk whose optical depth is greater towards the ring's periapse (Fig. 4). This asymmetry also persists out to great distances from the star, $r \sim 100$'s AU.
- This asymmetry is sensitive to both the dust size distribution q and the birth ring's eccentricity e_r (Fig. 5).
- An asymmetric debris disk also implicates perturbations from an unseen planet, since a planet's secular perturbations can readily sustain the birth ring's eccentricity (Chiang et al 2009).
- The debris disk orbiting Fomalhaut is particularly interesting, since its inner gap is eccentric, $e_r \simeq 0.1$, and is maintained by a known exoplanet (Kalas et al 2008). This system will be considered in a followup study.

Acknowledgments:
Support for this work was provided by NASA via a Hubble Theory/Archive grant from the Space Telescope Science Institute.

References

Chiang, Kite, Kalas, Graham, Clampins, 2009, ApJ, 693, 734.
Goldstein, 1980, in Classical Mechanics.
Golimowski, 42 coauthors, 2006, AJ, 131, 3109.
Krist, 40 coauthors, 2005, AJ, 129, 1008.
Strubbe, Chiang, 2006, ApJ, 648, 652.